


Flow Topology Transition via Global Bifurcation in Thermally Driven Turbulence

Yi-Chao Xie (谢毅超), Guang-Yu Ding (丁广裕), and Ke-Qing Xia (夏克青)

Department of Physics, The Chinese University of Hong Kong, Shatin, Hong Kong, China

 (Received 18 January 2018; revised manuscript received 22 March 2018; published 22 May 2018)

We report an experimental observation of a flow topology transition via global bifurcation in a turbulent Rayleigh-Bénard convection. This transition corresponds to a spontaneous symmetry breaking with the flow becomes more turbulent. Simultaneous measurements of the large-scale flow (LSF) structure and the heat transport show that the LSF bifurcates from a high heat transport efficiency quadrupole state to a less symmetric dipole state with a lower heat transport efficiency. In the transition zone, the system switches spontaneously and stochastically between the two long-lived metastable states.

DOI: [10.1103/PhysRevLett.120.214501](https://doi.org/10.1103/PhysRevLett.120.214501)

Large-scale flows (LSFs) in turbulence are ubiquitous in nature, e.g., oceanic currents and atmospheric flows. As the Reynolds number (Re) increases, a flow undergoes a sequence of spontaneous symmetry breakings, leading to different flow states, e.g., laminar flow, chaotic flow, etc. The broken symmetry is restored statistically for sufficiently high Re [1]. Fully developed turbulence may also exhibit transitions among different flow states characterized by different LSF topologies. Several recent studies in high Re turbulence systems, e.g., von Kármán swirling flow, Taylor-Couette flow and spherical Couette flow, indeed showed that the LSFs can exhibit multiple states [2–7], which contradicts the common understanding of turbulence suggested by Kolmogorov; i.e., there is only one state for high Re turbulence owing to the vigorous fluctuations [8]. However, in these examples, the transitions to multiple states are usually realized by explicitly changing the forcing symmetry of the system. In a rotating turbulent Rayleigh-Bénard convection (RBC), the heat transport exhibits a sequence of sharp transitions as the rotation rate increases [9–11]. Since Re is actually reduced with increasing rotation rate [12], the transitions observed in rotating RBC, therefore, occur as the flow becomes ostensibly less turbulent.

In this Letter, we present experimental evidences of flow topology transition from a high-symmetry state to a low-symmetry state via global bifurcation with the increase of turbulence level in thermally driven turbulence. The two states are characterized by different flow structures and distinctive heat transport efficiencies. This transition corresponds to a spontaneous symmetry breaking in a system far away from equilibrium. In the transition zone, the system exhibits stochastic switching between two long-lived metastable states. As spontaneous symmetry breaking is one of the unifying themes in modern physics, such as in particle and condensed matter physics; the present finding could thus be of interest to a wider range of fields beyond fluid dynamics.

Rayleigh-Bénard convection, where a fluid layer is confined between two horizontally parallel plates heated from below and cooled from above, is a well-known model system for studying thermally driven turbulence (for recent reviews on turbulent RBC, see, e.g., [13–17]). The experiment was carried out in an annulus convection cell. This geometry has been used in the studies of transition to spatial-temporal chaos [18–20]. The details of the experimental setup and measurement procedures are provided in the Supplemental Material [21]. Here, we describe only key features of the cell. The sidewalls of the cell were made up of two upright concentric Plexiglas cylinders. The outer cylinder had an inner radius of $R_o = 96$ mm, and the inner cylinder had an outer radius of $R_i = 84.5$ mm. The two cylinders had an equal height $H = 100.0$ mm and wall thickness of 3.0 mm. Thus, the radius ratio was $\gamma = R_i/R_o = 0.88$, and the aspect ratio was $\Gamma = 2R_o/H = 1.88$. The copper bottom plate was heated by a Nichrome wire heater embedded into carved grooves underneath. The copper top plate was cooled by temperature-controlled circulating water passing through a chamber fitted to its top surface. Respective temperatures of the top and the bottom plates were measured using six thermistors that were uniformly distributed along the azimuth. Deionized and degassed water was used as the working fluid. Special care was taken to ensure the system had a temperature stability better than 0.05 K and an excellent thermal isolation from the laboratory environment.

The flow is controlled by the Rayleigh number $Ra = \alpha g \Delta T H^3 / (\nu \kappa)$, which is the ratio between the driving buoyancy force and the dissipative forces, and the Prandtl number $Pr = \nu / \kappa$. Here, α , ν , and κ are, respectively, the thermal expansion coefficient, the kinematic viscosity, and the thermal diffusivity of the working fluid. These properties are evaluated at the mean temperature of the system. The applied temperature difference is ΔT , and the gravitational acceleration constant is g . The response of the system, i.e., the Nusselt number Nu which

measures the effective thermal conductivity, is given by $Nu = qH/(\chi\Delta T)$, with q the input heat flux at the bottom plate and χ the thermal conductivity of the fluid. The experiment was performed in the Ra range of $6.0 \times 10^7 \leq Ra \leq 1.3 \times 10^9$, where the bulk flow is in a fully developed turbulence state, as evidenced by the fact that the critical Ra for onset of convection for our annulus geometry is $Ra_c \approx 6 \times 10^3$ [22]. The Pr was fixed at 5.43 corresponding to a mean temperature of 30.0°C. For each Ra , the applied heat flux was kept at a constant, and the responses of the system, i.e., the Nu and the LSF dynamics, were measured simultaneously at a sampling rate of 0.43 Hz.

A multithermal-probe method was used to measure the flow dynamics, which has been shown to be very effective in turbulent convection experiments [23–26]. Since the LSF carries hot (cold) thermal plumes with temperatures higher (lower) than the azimuthally averaged value, its structure and dynamics can be detected by measuring the time series of temperature profile along the cell periphery. Two thermistor arrays were installed with respective distances $H/3$ and $2H/3$ from the bottom plate. Each of the arrays consisted of 12 thermistors inserted into blind holes uniformly distributed along the azimuth. These holes were drilled from outside into the outer sidewall of the cell with a distance of 0.7 mm between the thermistor head and the fluid-sidewall contact surface. The thermistors were calibrated separately and individually with an accuracy of better than 0.01 K. Correlation analysis shows that the flow dynamics probed at the two heights are essentially the same; we therefore present results based on the thermistor array at $H/3$ in the following. At each time step, the temperature profile was expanded using discrete Fourier series, i.e., $T(i) = T_0 + \sum_{n=1}^6 A_n \cos[(\pi/6)i + \theta_n]$ ($i = 1 \dots 12$), where A_n and θ_n are, respectively, the amplitude and the phase of the n th Fourier mode, and T_0 is the azimuthally averaged temperature. The structure and dynamics of the LSF were determined by the predominant Fourier mode from $A_n(t)$. It is found that the first and the second modes are the strongest, and together they account for about 80% of the total energy. As the transition occurs, the flow changes from the second mode being dominant in total energy to the first mode being dominant. Through analysis of θ_n , it is found that the entire LSF pattern meanders azimuthally but with a speed less than one-tenth of the azimuthal speed of the fluid. While the mean azimuthal orientation of the LSF pattern does not show any obvious dependence on Ra , it tends to be distributed over half of the azimuthal plane.

We begin by presenting results from the heat transport measurements. Figure 1 shows the compensated Nusselt number $Nu/Ra^{0.274}$ as a function of Ra . A sharp transition at $Ra^* \approx 6.35 \times 10^8$ is visible. Before this transition, the measured heat transport scaling, i.e., $Nu = (0.242 \pm 0.001)Ra^{0.274 \pm 0.003}$, is consistent with

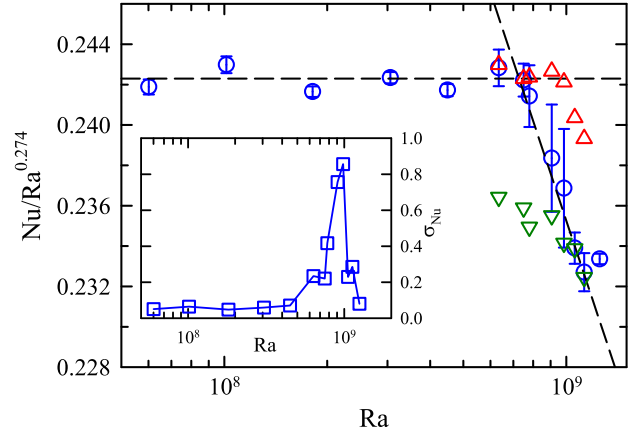


FIG. 1. Compensated Nu as a function of Ra (circles). The error bars represent the rms values σ_{Nu} , which are shown in the inset. The up-pointing triangles represent $\langle Nu \rangle_{A_2}$ (Nu averaged over periods when the quadrupole state is dominating), and the down-pointing triangles represent $\langle Nu \rangle_{A_1}$ (Nu averaged over periods when the dipole state is dominating), which are the average Nu weighted by the contributions from the respective flow states. The dashed lines are power law fits to the data.

measurements in other cell geometries within similar parameter range [27–29]. For $Ra > Ra^*$, the slope of Nu - Ra scaling drops sharply, with an exponent of 0.17 over the narrow Ra range. The error bars in the figure are based on the root-mean-square (rms) values of Nu that are shown in the inset. It is seen that σ_{Nu} remains very small before the transition, but it increases abruptly when Ra^* is approached, reaches a maximum at $Ra = 9.84 \times 10^8$, and then decreases to the level before the transition for the largest Ra explored.

To understand the transition and the enhanced Nu fluctuation, we study the dynamics of the LSF when Ra is increased. Two-dimensional horizontal velocity fields at different heights ($z/H = -0.36, -0.04, \text{ and } 0.45, z = 0$ at the mid-height of the cell) were measured by particle image velocimetry (PIV) with a camera placed above the convection cell and a horizontal laser sheet shone from the side. Detailed PIV measurement procedures are given in the Supplemental Materials [21]. To gain optical access, a transparent and thermally conductive sapphire disc was used as the top plate. The copper side shield was replaced with several layers of thermally insulating material with slits allowing laser-sheet access. At each height, 18 000 vector fields with a sampling rate of 15 Hz were acquired from which the mean flow field was obtained.

Figures 2(a) and 2(b) show the mean LSF structure at $Ra = 1.2 \times 10^8$ and $Ra = 1.1 \times 10^9$, respectively. The velocity field is color-coded using the azimuthal velocity component, with red for the clockwise direction and blue for the anticlockwise direction when viewed from the top. It is seen that the LSF exhibits a quadrupole structure or state (QS) for $Ra < Ra^*$ [Fig. 2(a)]; i.e., the locations of the two hot ascending regions and two cold descending regions of

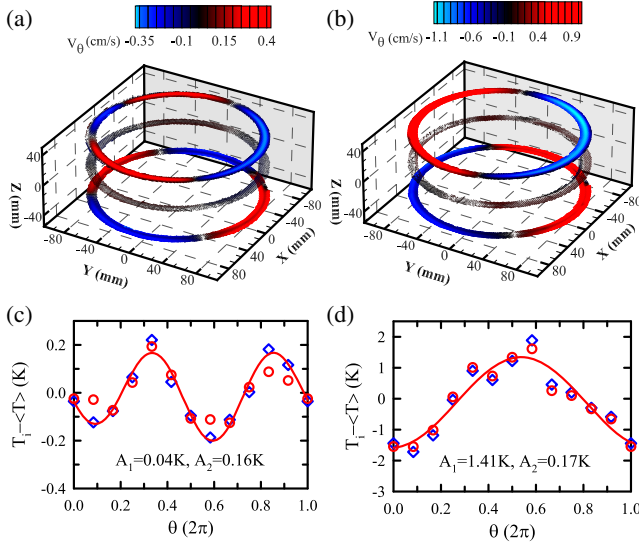


FIG. 2. (a),(b) Mean large-scale flow structure. (c),(d) Corresponding mean temperature profiles measured from the bottom plate (diamonds) for $Ra = 1.2 \times 10^8$ (left panel) and $Ra = 1.1 \times 10^9$ (right panel). In (a) and (b), the two-dimensional velocity fields at three horizontal planes ($z/H = -0.36, -0.04, \text{ and } 0.45$) are shown with the color bar representing the azimuthal velocity component (blue for anticlockwise direction and red for clockwise direction when viewed from the top). In (c) and (d), the lines are the fitting to the diamonds using the first two modes with A_1 and A_2 being their respective amplitudes. The circles are temperature profiles measured in the sidewall. See text for details.

the LSF appear alternatively along the azimuthal direction and the LSF shows a dipole structure or state (DS) for $Ra > Ra^*$, i.e., the rising hot plumes and the falling cold plumes of the LSF are separated by $\sim \pi$ azimuthally. Note that the former flow pattern has higher symmetry than the latter one.

Figures 2(c) and 2(d) show the time averaged azimuthal temperature profiles, where the diamonds were measured from the bottom plate (with 12 embedded thermistors) and acquired simultaneously with the PIV measurement. The circles were measured from the sidewall at $z = H/3$, with the copper top plate and with the copper side shield in place. The lines are the fits to the diamonds using the first and the second Fourier modes which yield $A_1 = 0.04$ K and $A_2 = 0.16$ K, and $A_1 = 1.41$ K and $A_2 = 0.17$ K, respectively. With A_2 being four times larger than A_1 in (c), the flow is dominated by the QS. In contrast, A_1 is eight times larger than A_2 in (d), suggesting that the mean flow is a DS. We thus see excellent agreement between results from the PIV and the multithermal-probe methods. It is also seen that the profiles measured from the sidewall (with the side shield present) and from the bottom plate (without the side shield) agree with each other excellently. This shows that the LSF pattern is quite robust under different thermal insulations. The excellent agreement between the two profiles measured at different heights (inside the bottom

plate and in the sidewall) also demonstrates that the LSF is highly coherent vertically, confirming the PIV results. [Note that due to the slightly different Ra for the two measurements shown in Fig. 2(c) ($Ra = 1.2 \times 10^8$ for diamonds and $Ra = 1.0 \times 10^8$ for circles), the amplitudes for the two profiles are somewhat different.]

Taking advantage of the long-time measurement capability of the multithermal-probe method, we now examine the long-term dynamics of the LSF. The evolution of the flow with increasing turbulence level is studied by mapping the flow state at each time instance onto a two-dimensional phase space constructed using $A_1/\Delta T$ and $A_2/\Delta T$. The trajectories of the LSF state in a so-constructed phase space for several typical values of Ra are shown in Figs. 3(a–e). For $Ra < Ra^*$ [Fig. 3(a)], the data points are confined in the region of small values of A_1 , indicating that the turbulent flow is dominated by the QS. They start to escape from the QS occasionally as Ra is increased [Fig. 3(b)]. In this parameter range, the flow stays in the QS most of the time. But occasionally it is kicked out by the vigorous turbulent fluctuations and reaches the DS. When Ra is further increased, the flow starts to switch between the QS and DS stochastically [Fig. 3(c)]. This leads to the observation of long-lived metastable states to be discussed below. The flow continues to evolve with increasing Ra . It is in the DS most of the time and occasionally escapes from it [Fig. 3(d)]. At the highest Ra reached in the experiment, the flow is totally trapped in the DS [Fig. 3(e)]. Thus, Figs. 3(a)–3(e) demonstrate dynamically how the transition from one LSF structure to the other occurs via a global bifurcation arising from spontaneous symmetry breaking as the turbulence level increases. Figure 3(f) shows the time fraction when the QS is dominating (τ_{QS} , circles) and that when the DS is dominating (τ_{DS} , triangles). Consistent with the scenario obtained from Figs. 3(a)–3(e), τ_{DS} is close to zero for small Ra and increases to one for the largest Ra achieved, whereas τ_{QS} is close to one for small Ra and

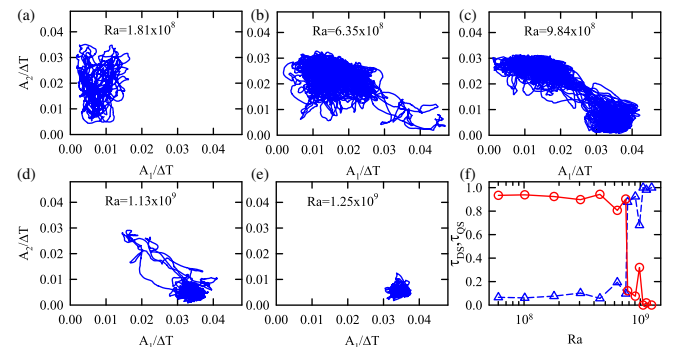


FIG. 3. (a)–(e) Trajectories of the large-scale flow state in a two-dimensional phase space constructed using $A_1/\Delta T$ and $A_2/\Delta T$, showing the evolution of the LSF with increasing Ra . (f) Time fraction when the quadrupole state is dominating (τ_{QS} , circles) and that when the dipole state is dominating (τ_{DS} , triangles) vs Ra .

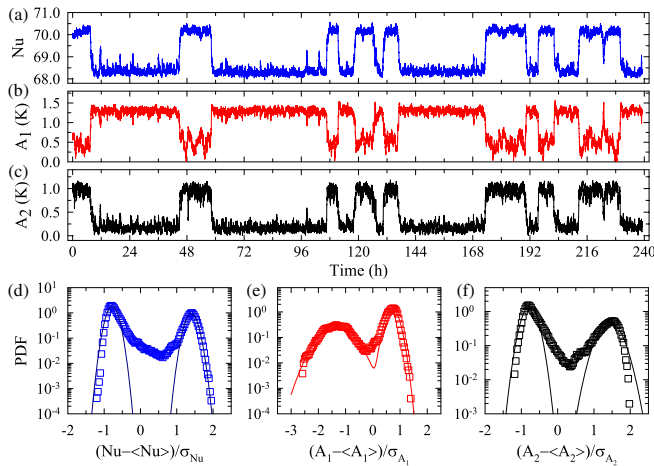


FIG. 4. Time series of (a) Nu , (b) A_1 , and (c) A_2 at $Ra = 9.84 \times 10^8$. The probability density functions (PDFs) of standardized Nu , A_1 , and A_2 are plotted in (d)–(f), respectively. The solid lines in (d)–(f) represent the two-Gaussian-function fit to the data.

decreases to zero after the transition. Note that there seems to be a sharp transition in τ for Ra around 8×10^8 , which is due to insufficient measurement time for the related data points.

We now examine in detail the flow dynamics and heat transport in the transition zone when the LSF switches between the QS and DS. Figures 4(a)–4(c) show, respectively, 240-hour time series of Nu , A_1 , and A_2 measured at $Ra = 9.84 \times 10^8$. It is seen that the time series of Nu , A_1 , and A_2 all exhibit two distinct levels corresponding to the QS and the DS. Random switchings between these two metastable states with distinctively different heat transport efficiencies are apparent. Nu is higher when A_2 is dominating than when A_1 is dominating [Fig. 4(a)], with the difference in Nu between the two states being $\sim 2.7\%$. It is well known that the primary heat carriers in turbulent convection are the thermal plumes [30]. Therefore, that the QS has a higher heat transfer efficiency than the DS may be attributed to the fact that the QS has twice the plume emission and impinging spots of those of the DS, as can be clearly seen from Figs. 2(a) and 2(b) (the region with zero azimuthal velocity in the top and bottom parts of the cell corresponds to the region where thermal plumes descending or ascending). The probability density functions (PDFs) of the standardized Nu , A_1 , and A_2 are plotted in Figs. 4(d)–4(f). The solid lines in (d)–(f) are fittings to the data using the sum of two Gaussian functions. Consistent with bistabilities shown in Figs. 4(a)–4(c), these PDFs exhibit bimodal distributions with double Gaussian peaks. The flow switching between two states with different Nu explains the greatly enhanced Nu fluctuation as seen in the inset of Fig. 1, where σ_{Nu} peaks at $Ra = 9.84 \times 10^8$.

Stochastic switching between flow states like the one shown in Fig. 4 are observed for all values of Ra within the

transition zone, i.e., for $6.35 \times 10^8 \leq Ra \leq 1.13 \times 10^9$. The global heat transport behavior within this range can be understood in terms of this switching. In Fig. 1, we also plot the Nu averaged over time period when A_1 is dominating and that when A_2 is dominating, denoted by $\langle Nu \rangle_{A_1}$ (down-pointing triangles) and $\langle Nu \rangle_{A_2}$ (up-pointing triangles), respectively. At the low- Ra end of the transition zone, the value of Nu averaged over the whole measurement period is seen to be almost the same as that of $\langle Nu \rangle_{A_2}$, consistent with the fact that the flow is dominated by the QS state for almost the entire measurement period, while at the high- Ra end of the transition zone, the value of Nu is almost the same as that of $\langle Nu \rangle_{A_1}$. After the transition, the system ends up in a lower symmetry state with lower heat transport efficiency.

Figure 4 also shows that the two metastable states are long lived, lasting as long as many hours, which are much longer than the typical turnover time of the LSF (on the order of a minute). For the example shown in Fig. 4, the average life time of the QS is 9.4 hours and that of the DS is 17.7 hours. Transitions between different flow states have been reported previously in turbulent thermal convection, i.e., the transition of the LSF between the single-roll mode and the vertically stacked double-roll mode [25,26,31]. However, those transitions exist for all values of Ra in the experiments, and the time the system spends in one state is on the order of the LSF turnover time. Moreover, none of the related quantities exhibit bimodal distribution. Therefore, the present observation contrasts sharply with those previous studies and suggests that the underlying dynamics governing those transitions are different from the present one.

In summary, we have demonstrated experimentally in thermally driven turbulence the existence of a flow topology transition via global bifurcation from a high-symmetry state to a low-symmetry state with distinctive heat transport efficiencies, i.e., a transition of the LSF structure from a quadrupole state to a dipole state. This transition is reminiscent of a spontaneous symmetry breaking in a system far away from equilibrium and with strong fluctuations. Moreover, it is shown that the state with higher symmetry is more efficient in heat transport. Within the transition zone of about one-half decade in Ra , the LSF shows spontaneous and stochastic switching between two long-lived metastable states.

A hallmark of fluid turbulence is the existence of an extremely large number of degrees of freedom. The formation of LSFs may simplify the description of turbulent flows. Instead of taking into account all the high-dimensional space, one can capture the essential LSF dynamics by considering only a few relevant flow modes and model the others stochastically. By applying the dynamical systems approach, turbulence may be described and even predicted in a much simpler way. Progresses have been made for turbulent swirling flows [2] and two-dimensional weak turbulence [32]. The present findings

should stimulate more studies of turbulent flows from the dynamical systems point of view, which should also have implications beyond fluid dynamics.

We thank R. Benzi, B. Dubrulle, D. Faranda, Y.-B. Hu, S.-D. Huang, C. Sun, and H.-D. Xi for useful discussions. This work was supported by the Hong Kong Research Grants Council (RGC) under Project No. CUHK14301115 and a National Science Foundation of China (NSFC) and Hong Kong RGC Joint Research Grant with Project No. N_CUHK437/15.

-
- [1] U. Frisch and A.N. Kolmogorov, *Turbulence: The Legacy of A. N. Kolmogorov* (Cambridge University Press, Cambridge, England, 1995).
- [2] D. Faranda, Y. Sato, B. Saint-Michel, C. Wiertel, V. Padilla, B. Dubrulle, and F. Daviaud, Stochastic Chaos in a Turbulent Swirling Flow, *Phys. Rev. Lett.* **119**, 014502 (2017).
- [3] S.G. Huisman, R.C.A. van der Veen, C. Sun, and D. Lohse, Multiple states in highly turbulent Taylor-Couette flow, *Nat. Commun.* **5**, 3820 (2014).
- [4] D.S. Zimmerman, S.A. Triana, and D.P. Lathrop, Bistability in turbulent, rotating spherical Couette flow, *Phys. Fluids* **23**, 065104 (2011).
- [5] P.P. Cortet, A. Chiffaudel, F. Daviaud, and B. Dubrulle, Experimental Evidence of a Phase Transition in a Closed Turbulent Flow, *Phys. Rev. Lett.* **105**, 214501 (2010).
- [6] A. de la Torre and J. Burguete, Slow Dynamics in a Turbulent von Kármán Swirling Flow, *Phys. Rev. Lett.* **99**, 054101 (2007).
- [7] F. Ravelet, L. Marié, A. Chiffaudel, and F. Daviaud, Multistability and Memory Effect in a Highly Turbulent Flow: Experimental Evidence for a Global Bifurcation, *Phys. Rev. Lett.* **93**, 164501 (2004).
- [8] A.N. Kolmogorov, The local structure of turbulence in incompressible viscous fluid for very large Reynolds numbers, *Dokl. Akad. Nauk SSSR* **30**, 299 (1941).
- [9] R. J. A. M. Stevens, J.-Q. Zhong, H. J. H. Clercx, G. Ahlers, and D. Lohse, Transitions between Turbulent States in Rotating Rayleigh-Bénard Convection, *Phys. Rev. Lett.* **103**, 024503 (2009).
- [10] S. Weiss, R. J. A. M. Stevens, J.-Q. Zhong, H. J. H. Clercx, D. Lohse, and G. Ahlers, Finite-Size Effects Lead to Supercritical Bifurcations in Turbulent Rotating Rayleigh-Bénard Convection, *Phys. Rev. Lett.* **105**, 224501 (2010).
- [11] P. Wei, S. Weiss, and G. Ahlers, Multiple Transitions in Rotating Turbulent Rayleigh-Bénard Convection, *Phys. Rev. Lett.* **114**, 114506 (2015).
- [12] S. Chandrasekhar, *Hydrodynamic and Hydromagnetic Stability*, Dover Books on Physics Series (Dover Publications, New York, 1961).
- [13] E. D. Siggia, High Rayleigh number convection, *Annu. Rev. Fluid Mech.* **26**, 137 (1994).
- [14] G. Ahlers, S. Grossmann, and D. Lohse, Heat transfer and large-scale dynamics in turbulent Rayleigh-Bénard convection, *Rev. Mod. Phys.* **81**, 503 (2009).
- [15] D. Lohse and K.-Q. Xia, Small-scale properties of turbulent Rayleigh-Bénard convection, *Annu. Rev. Fluid Mech.* **42**, 335 (2010).
- [16] F. Chillá and J. Schumacher, New perspectives in turbulent Rayleigh-Bénard convection, *Eur. Phys. J. E* **35**, 58 (2012).
- [17] K.-Q. Xia, Current trends and future directions in turbulent thermal convection, *Theor. Appl. Mech. Lett.* **3**, 052001 (2013).
- [18] S. Ciliberto and P. Bigazzi, Spatiotemporal Intermittency in Rayleigh-Bénard Convection, *Phys. Rev. Lett.* **60**, 286 (1988).
- [19] P. Kolodner, D. Bensimon, and C.M. Surko, Traveling-Wave Convection in an Annulus, *Phys. Rev. Lett.* **60**, 1723 (1988).
- [20] F. Daviaud, M. Bonetti, and M. Dubois, Transition to turbulence via spatiotemporal intermittency in one-dimensional Rayleigh-Bénard convection, *Phys. Rev. A* **42**, 3388 (1990).
- [21] See Supplemental Material at <http://link.aps.org/supplemental/10.1103/PhysRevLett.120.214501> for details of the experimental setup and measurement procedures.
- [22] B.-F. Wang, Z.-H. Wan, D.-J. Ma, and D.-J. Sun, Rayleigh-Bénard convection in a vertical annular container near the convection threshold, *Phys. Rev. E* **89**, 043014 (2014).
- [23] S. Cioni, S. Ciliberto, and J. Sommeria, Strongly turbulent Rayleigh-Bénard convection in mercury: comparison with results at moderate Prandtl number, *J. Fluid Mech.* **335**, 111 (1997).
- [24] E. Brown, A. Nikolaenko, and G. Ahlers, Reorientation of the Large-Scale Circulation in Turbulent Rayleigh-Bénard Convection, *Phys. Rev. Lett.* **95**, 084503 (2005).
- [25] H.-D. Xi and K.-Q. Xia, Flow mode transitions in turbulent thermal convection, *Phys. Fluids* **20**, 055104 (2008).
- [26] Y.-C. Xie, P. Wei, and K.-Q. Xia, Dynamics of the large-scale circulation in high-Prandtl-number turbulent thermal convection, *J. Fluid Mech.* **717**, 322 (2013).
- [27] T. Y. Chu and R. J. Goldstein, Turbulent convection in a horizontal layer of water, *J. Fluid Mech.* **60**, 141 (1973).
- [28] K.-Q. Xia and S.-L. Lui, Turbulent Thermal Convection with an Obstructed Sidewall, *Phys. Rev. Lett.* **79**, 5006 (1997).
- [29] X.-L. Qiu and K.-Q. Xia, Viscous boundary layers at the sidewall of a convection cell, *Phys. Rev. E* **58**, 486 (1998).
- [30] X.-D. Shang, X.-L. Qiu, P. Tong, and K.-Q. Xia, Measured Local Heat Transport in Turbulent Rayleigh-Bénard Convection, *Phys. Rev. Lett.* **90**, 074501 (2003).
- [31] S. Weiss and G. Ahlers, Turbulent Rayleigh-Bénard convection in a cylindrical container with aspect ratio $\Gamma = 0.50$ and Prandtl number $Pr = 4.38$, *J. Fluid Mech.* **676**, 5 (2011).
- [32] B. Suri, J. Tithof, Roman O. Grigoriev, and M. F. Schatz, Forecasting Fluid Flows Using the Geometry of Turbulence, *Phys. Rev. Lett.* **118**, 114501 (2017).